


Article

Ultrasonic–Thermal Regeneration of Spent Powdered Activated Carbon

Tingting Zhang ^{1,2,*}, Yanling Yang ³, Xing Li ³, Zhiwei Zhou ³  and Bigui Wei ^{1,2}

¹ School of Environmental and Municipal Engineering, Lanzhou Jiaotong University, Lanzhou 730070, China; weibg@mail.lzjtu.cn

² Key Laboratory of Yellow River Water Environment in Gansu Province, Lanzhou 730070, China

³ Faculty of Architecture, Civil and Transportation Engineering, Beijing University of Technology, Beijing 100124, China; yangyanling@bjut.edu.cn (Y.Y.); lixing@bjut.edu.cn (X.L.); hubeizhouzhiwei@163.com (Z.Z.)

* Correspondence: zhangting1229ztt@163.com

Abstract: This study investigated the ultrasonic–thermal regeneration of powdered activated carbon (PAC) spent using 4-chlorophenol (4-CP). Similarly, a thermal regeneration process was also studied and the reaction conditions (i.e., regeneration temperature, heating rate, regeneration time) were tested. Fourier transform infrared spectroscopy (FT-IR), thermogravimetric analysis (TGA), scanning electron microscopy (SEM), X-ray photoelectron spectroscopy (XPS) and X-ray diffraction (XRD) analysis were applied to characterize the regenerated PACs under different treatments (thermal, ultrasonic and ultrasonic–thermal) and also compare them with the fresh and exhausted PACs. According to our regeneration observations, the ideal regeneration parameters were determined to be a 40 kHz frequency, 0.18 W/mL sonication power, 0.1 M NaOH and 50% (*v/v*) ethyl alcohol as the regeneration solution, and 1 g/L of saturated PAC mass with thermal regeneration as the second stage at 500 °C, desorbed for 30 min with a heating rate of 20 °C min^{−1}. Under these conditions, the RE value achieved 90.99% and the η value reached 5.6%. The results of FTIR, XPS and XRD revealed that the oxygen functional group content of ultrasonic–thermal regenerated PAC significantly increased. These oxygenous groups exerted a positive effect on the adsorption process of the regenerated PAC and the subsequent adsorption–regeneration process.

Keywords: ultrasonic; thermal; regeneration; powdered activated carbon; characteristic



Citation: Zhang, T.; Yang, Y.; Li, X.; Zhou, Z.; Wei, B. Ultrasonic–Thermal Regeneration of Spent Powdered Activated Carbon. *Sustainability* **2023**, *15*, 9060. <https://doi.org/10.3390/su15119060>

Academic Editors: Maurizio Volpe, Amir Mahboubi Soufiani and Taner Sar

Received: 20 April 2023

Revised: 25 May 2023

Accepted: 1 June 2023

Published: 3 June 2023



Copyright: © 2023 by the authors. Licensee MDPI, Basel, Switzerland. This article is an open access article distributed under the terms and conditions of the Creative Commons Attribution (CC BY) license (<https://creativecommons.org/licenses/by/4.0/>).

1. Introduction

The application of powder activated carbon (PAC) for the adsorption of organic contaminants is an effective and reliable water treatment method. Activated carbon is considered to be an excellent adsorbent, especially in the presence of phenolic compounds [1–4]. When PAC is saturated, it becomes a residue that must be eliminated and replaced with fresh PAC. Therefore, the financial viability of PAC’s extensive commercial application depends on both its high-efficiency regeneration and the cost of producing PAC. Considering the significance of the activated carbon regeneration process, various regeneration techniques of saturated PAC have been proposed [5–12], such as physicochemical regeneration [5], Fenton-like oxidation regeneration [6], electrochemical regeneration [7,9], ozonation regeneration [10], bio-regeneration [12] and ultrasound regeneration [13]. As for the various regeneration procedures, thermal regeneration is regarded as the most economically advantageous approach [14–20].

The adsorption capability of activated carbon exhibits an excellent recovery that is reported in the literature; the analyses show that during the thermal regeneration process, the loss of activated carbon is very great [14]. The environment is also threatened by intermediate byproducts such as SO₂ that are generated through the thermal regeneration process.

The ultrasonic regeneration of PAC is a new and effective method of adsorbent regeneration. Waves are dampened during ultrasonic propagation by cavitation bubbles and absorption in the aqueous phase. The phenomenon of cavitation happens as ultrasonic waves travel through a liquid medium. Owing to the great intensity of sound waves, tiny gas bubbles are formed to overcome the liquid's traction resistance. When the bubbles reach a crucial size, they collapse and produce a significant quantity of power [21,22]. The energy produced in the process of ultrasound can generate the following consequences: Firstly, local temperature significantly rises in areas known as "hot spots". Secondly, high-pressure shock waves are formed. Thirdly, high-speed microjets are generated that release at hundreds of km h^{-1} and react on the material's surface [23,24]. Ultrasonic cavitation is significantly affected by the frequency and intensity of ultrasound, thus influencing the size of the cavitation bubble. At low frequencies, the bubble size might increase. Increased intensity prevents bubble growth by causing early collapses. When an ultrasonic wave is introduced into the liquid phase, small cavitation bubbles are produced. When the cavitation bubbles grow to a critical size, they collapse and release a large amount of energy into the aqueous phase. During the regeneration process, ultrasound can lead to the disintegration of the adsorbates. Pollutant degradation mechanisms are significantly related to the frequency of ultrasound. For low ultrasonic frequencies (20–100 kHz), desorption as a result of the mechanical impact of sound irradiation is dominant. The chemical effects become more significant at high frequencies (300–800 kHz). In this case, the hydroxyl ions formed in the liquid medium and subsequently the adsorbate are degraded [16]. By using a low frequency and considerable power, the cavitation effects increase and the desorption efficiency improves. Moreover, results show that desorption at a low frequency (20 kHz) can be carried out with little mass loss [25].

As can be seen, ultrasonic cavitation on the local surface of activated carbon generates local high temperatures, high pressures, high-speed liquid microjets and other extreme physical reactions that can strengthen the desorption process, creating a localized high-temperature thermal regeneration environment on the surface of the PAC that has the characteristics and efficiency of high-temperature thermal regeneration.

In our previous work [26], we investigated the ultrasonic desorption of PAC spent with 4-chlorophenol (4-CP). We found that under optimized regenerated conditions, the regeneration efficiency achieved 86.81%. This project aims to take this research one step further. Here, we investigated the regeneration efficiency of thermal regeneration and ultrasonic–thermal combination technology in the desorption of saturated PAC. The interface characteristics of various PACs under different regeneration conditions were analyzed. The regeneration potential of ultrasonic–thermal combination technology for saturated PAC was also comprehensively evaluated. Our research results provide meaningful guidance for further development of ultrasonic regeneration and could significantly reduce the energy consumption of traditional thermal regeneration.

2. Materials and Methods

2.1. Chemicals and Reagents

All reagents were of analytical grade 4-CP (99%); sodium hydroxide (NaOH, $\geq 98\%$) and PAC (100 mesh) were supplied by Aladdin (Shanghai, China). The features of the PAC included the following: specific area $1156 \text{ m}^2/\text{g}$, average pore size 2.62 nm , micro-pore volume $0.21 \text{ cm}^3/\text{g}$, meso-pore and macro-pore volume $0.45 \text{ cm}^3/\text{g}$, iodine number 967.35 mg/g , and methylene blue adsorption 236.56 mg/g . Ethyl alcohol ($\text{CH}_3\text{CH}_2\text{OH}$, $\geq 99.7\%$) was acquired from Sinopharm Chemical Reagent (Beijing, China). The basic solutions were produced using water purified using a Millipore purification system (Milli-Q Advantage A10, Millipore, Burlington, MA, USA). The fresh PAC was cleaned with Milli-Q deionized water and then boiled four times. The cleaned PAC was put in an oven at $105 \text{ }^\circ\text{C}$ to a consistent weight, then placed in a desiccator.

2.2. Regeneration Experimental Procedures

We mixed 1 g of pretreatment, cleaned PAC with 1000 mL of 100 mg/L 4-CP solution until the PAC completely reached saturation. Before conducting the desorption tests, the suspension was maintained at room temperature (25 ± 2 °C) with stirring at 300 rpm for two days to establish equilibrium. The spent PAC was weighed and stored in a desiccator for further regeneration after being dried at 90 °C for 12 h.

Two stages of batch regeneration tests were conducted:

- (1) The first steps were carried out under isothermal settings (exploring the impact of temperatures between 300 and 700 °C) and dynamical heating conditions (exploring the influence of heating rate between 20 and 40 °C min⁻¹).
- (2) Second-step procedures: When prior experiences made it possible to determine the appropriate situations for a higher-adsorption-capacity recovery, the obtained thermal regenerated PAC was then regenerated in an ultrasonic cleaner under an optimal condition that we reported in previous work [26] (with 40 kHz frequency, 0.18 W/mL sonication intensity, 0.1 M NaOH and 50% (v/v) ethyl alcohol mixture as the regeneration solution, and 1 g/L of saturated PAC mass determined to be the optimal desorption conditions).

2.3. Analytical Methods

Using a high-temperature TGA/DSC synchronous thermal analyzer (TGA/DSC 1, METTLER-TOLEDO, Zurich, Switzerland), thermogravimetric analysis was conducted. For each test, 5 mg of PAC was exposed to heat at a rate of 10 K/min from 30 °C to 800 °C in argon surroundings (50 mL/min). The chemical functional groups were determined qualitatively via FTIR (V70/HYPERION 1000, Bruker, Billerica, MA, USA). All spectra were within the wavenumber range of 4000 and 400 cm⁻¹. Scanning electron microscopy (SEM, SU-8020, Hitachi, Tokyo, Japan) was applied to analyze the surface morphology of the original, saturated and regenerated PACs. X-ray diffraction (XRD, D8 Advance, Bruker, Karlsruhe, Germany) was applied to describe the crystal structure of the fresh and the regenerated PACs using Cu-K radiation in the range of 2θ from 10 to 80°. By using an X-ray photoelectron spectrometer (XPS, ESCALAB 250Xi, Thermo Fisher, Waltham, MA, USA), the chemical constitutions of the test samples were investigated.

The concentrations of the 4-CP were measured using HPLC (Agilent 1260 LC, Agilent, Santa Clara, CA, USA), and the mobile phase for the 4-CP was ultrapure water containing 0.2% acetic acid/MeOH (40:60, v/v). Detection was performed at 278 nm.

The regeneration efficiency (RE, %) and the weight loss percentage (η, %) were determined according to Equations (1) and (2).

$$RE(\%) = \frac{\text{adsorption capacity of regenerated PAC}}{\text{adsorption capacity of fresh PAC}} \times 100 \quad (1)$$

$$\eta(\%) = \frac{W_t}{W_0} \times 100 \quad (2)$$

where η is the weight loss percentage of PAC, while the weights of PAC prior to desorption and subsequent to regeneration are W_0 and W_t , respectively.

3. Results and Discussion

3.1. Thermal Desorption Efficiency of Saturated PAC

3.1.1. Effect of Regeneration Temperature

The influence of regeneration temperature was investigated between 300 and 700 °C. Figure S1 displays the effect of regeneration temperature on the RE value at regeneration times of 30 min and 60 min. As observed, the RE value was significantly promoted with a higher regeneration temperature. The RE increased from 63.89% to 85.91% and 78.60% to 90.54% as the regeneration temperature was raised from 300 to 700 °C, respectively. The activation energy for the carbon–steam reaction would typically decline with an improve-

ment in regeneration temperature, resulting in a promotion in reaction rate and a higher RE value. The adsorption process of 4-CP on PAC is mainly chemical adsorption. With the increase in regeneration temperature, the corresponding chemical bonds between 4-CP and PAC's surface functional groups break. The results that appear here were consistent with trends that are frequently observed during pyrolysis procedures. At a higher temperature, the 4-CP molecules are pyrolyzed to produce small molecular compounds. The small molecular compounds are easy to volatilize and desorb from PAC, which further improved the regeneration rate of PAC. In the same way that a high temperature promoted the expansion of pore structure [20], it also accelerated the cracking processes of the chemisorbed percentage for exhausted carbons. Márquez et al. reported that thermal regeneration at temperatures no higher than 350 °C can be a simple and sustainable alternative to recover GAC used in WWTPs, with regeneration efficiencies reaching (72–98%) [18].

3.1.2. Effect of Heating Rate

Figure 1 shows the results of RE value and η value at different heating rates for the runs made in a series of tests. The results show that a higher heating rate led to a higher RE of PAC, Figure 1a. For two certain regeneration temperatures, 500 °C and 700 °C, when the heating rate changed from 20 °C min⁻¹ to 40 °C min⁻¹, the related RE values increased from 86.82% to 89.16% and from 90.22% to 99.88%. The findings demonstrate that the desorption of 4-CP from PAC is facilitated by an increase in heating rate at 700 °C. The 4-CP molecules are easy to desorb from the pores of PAC due to rapid thermal decomposition during the process of a rapid temperature rise stage. Figure 1b exhibits the value of η at various heating rates. The value of η was remarkably increased with the improvement in heating rate. For example, η was 7.7% for 20 °C min⁻¹, after which it increased to 9.7% for 40 °C min⁻¹ at a temperature of 500 °C. The value of η at 500 °C is significantly lower than that at 700 °C. These results are due to the fact that a faster heating rate increases energy transfer and also reduces the time spent in residence by gases, which causes the desorption of the byproducts to degrade. At high temperatures, the decomposition of organics is accelerated and some small molecular substances are produced; additionally, some PAC is carbonized. Thus, the value of η increases.

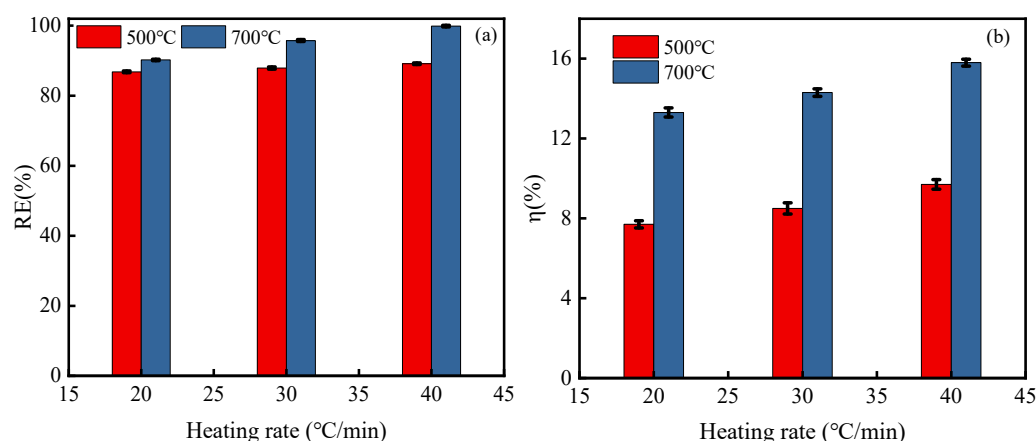


Figure 1. Effects of heating rate on PAC regeneration rate (a) and PAC mass loss rate (b).

3.1.3. Effect of Regeneration Time

With a regeneration temperature of 500 °C and a heating rate of 20 °C min⁻¹, Figure S2 illustrates the effect of regeneration times on the RE and η values with times ranging from 30 to 90 min. It is obvious that the RE increased from 75.98% to 98.45% as the regeneration time increased from 30 to 90 min, along with an increase in η value from 7.1% to 8.7%. Extending the regeneration time is favorable for the desorption of 4-CP from PAC. However, a longer regeneration time results in a greater PAC weight loss percentage. Therefore, it is necessary to choose a suitable regeneration time to achieve the desired result. Here,

we chose a regeneration time of 60 min. Additionally, a deep recovery of the adsorbent capacity needs an extreme temperature, resulting in a larger weight loss for the PAC. This result is consistent with the thermogravimetric analysis described in Section 3.3.2.

3.2. Ultrasound-Enhanced Thermal Regeneration Efficiency of Saturated PAC

3.2.1. PAC Regeneration Rate

The PAC regeneration rate under different regeneration temperatures of the thermal combined ultrasonic regeneration process is shown in Figure 2. It is noticeable that the RE value initially grew with regeneration temperature, then gradually increased, with final RE values reaching 95.56% and 99.65% for regeneration times of 30 min and 60 min, respectively, at 700 °C. The adsorption capacity was almost up to the initial value of the fresh adsorbent. Compared with the RE value of 700 °C after 30 min and 60 min, increasing the regeneration time obviously improved the adsorption process. Interestingly, the RE value is independent of time, twice the regeneration time but the RE value was almost the same as the level obtained with 30 min. The RE value for only thermal regeneration at 700 °C for 30 min was 85.91%, while the RE value was 86.81% for only ultrasonic regeneration after 180 min. We observed that the RE value obtained from thermal–ultrasound treatment at 500 °C for 30 min reached 90.99%. This result confirms that ultrasonic regeneration as a pretreatment can reduce the temperature required for thermal regeneration. In addition, the RE value increased by 10.09% at 700 °C for 30 min. This was due to the cavitation bubbles produced by the ultrasound wave growing and collapsing to form high-pressure micro-jets, a high-temperature local environment and a limited number of ·OH radicals, which together promote the desorption procedure of 4-CP molecules from PAC [27,28]. In addition, the pore structure of the carbon also contributed to the desorption of the carbon. As reported, the particle size of activated carbon became smaller, the porosity recovered better and the surface area value increased after ultrasound regeneration [29]. Ultrasound also enhanced surface diffusion of PAC. For the above reasons, the heating temperature were reduced and the regeneration time for the subsequent thermal regeneration process were saved.

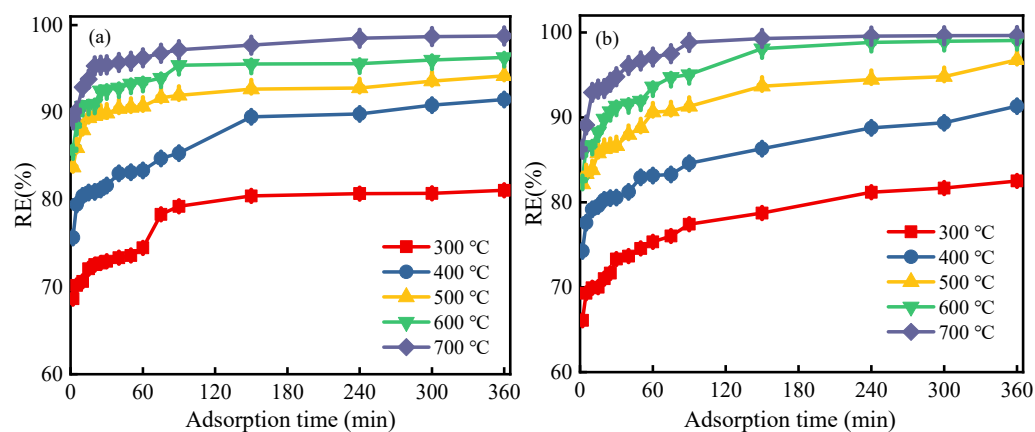


Figure 2. Effect of ultrasonic–thermal regeneration on PAC regeneration rate: (a) regeneration time 30 min; (b) regeneration time 60 min.

3.2.2. PAC Weight Loss Percentage

Figure 3 illustrated the weight loss percentage (η , %) of various regeneration methods. Obviously, an improvement in the regeneration temperature would facilitate the value of η . It should be noted that the values of η for ultrasonic–thermal treatment after 30 min and 60 min were both lower than that for single thermal regeneration. For example, when under the temperature of 500 °C and regenerated for 30 min, the value of η for the ultrasonic–thermal process decreased by 21.13% compared with single thermal regeneration. The results above demonstrate that ultrasonic–thermal combined regeneration can markedly reduce the weight loss of PAC, and energy consumption for heating can also be reduced. This

can be explained by the following reasons: (i) The turbulence and shock wave generated by ultrasound cavitation accelerated the mass transfer process among the solid surface of PAC and the liquid phase, which is the main mechanism of heterogeneous acoustic chemical reactions [30]. (ii) The mechanical effect and cavitation effect of ultrasound cleared the pores blocked in the saturated PAC [31–33], which created superior regeneration conditions for the following thermal desorption, reducing the weight loss of PAC.

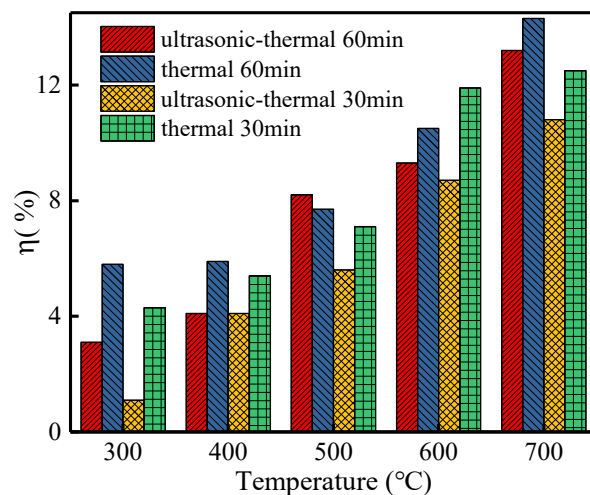


Figure 3. Effect of ultrasonic-enhanced thermal regeneration on PAC mass loss rate.

3.3. Characteristics of PACs with Different Regeneration Methods

3.3.1. FTIR Analysis

The spectra of FTIR for initial, exhausted and various regenerated PAC tests are represented in Figure 4. Various sources published the assignments of the respective functional groupings [19,34–36]. For the initial-PAC, the O–H stretching vibrations of the hydroxyl groups in phenols, alcohols and carboxylic acids are responsible for an absorption peak at 3200 cm^{-1} . This peak disappeared after three regeneration process, illustrating that during the regeneration process, the O–H band was broken. The broad band between 3676 to 3424 cm^{-1} indicates the presence of H–O–H, which is correlated with the presence of water molecules on the PAC surface. There are noticeable distinctions in sample peak location. As for the ultrasonic–thermal–PAC, the peaks were various. The location at 1740 cm^{-1} was recognized to indicate the existence of C=O stretching in carboxyl. Compared to the ultrasonic–PAC and thermal–PAC, the peak at 1740 cm^{-1} was weakened. We speculate that the C=O group in carboxyl was produced during the thermal combined ultrasonic process. The band that exists at 1580 cm^{-1} is notable due to the fact that it is connected to C=O vibrations in aromatic rings and carbonyl compounds. The aromatic C=C stretches in phenyl were related to the peak at 1427 cm^{-1} . The above spectral differences are caused by differences in temperature. However, despite this difference, many inflections or peaks can be observed in different spectra, suggesting differences in the desorption of various molecular species caused by ultrasonic effects, not only temperature. Peaks around 1219 cm^{-1} and 867 cm^{-1} were attributed to the stretching of C–O groups in phenol and Ar–H out-of-plane bending in phenyl groups, respectively. The peak at 1069 cm^{-1} is associated with the out-of-plane bending of aromatic C–H bonds. It should be noted that the average spectrum of Thermal-PAC was narrow compared to all samples, which demonstrates that thermal treatment mainly contributed to the physical desorption of 4-CP. The declines in surface-oxygen-containing groups were not conducive to improvement in adsorption capacity for regenerated PAC. This result is also consistent with the findings reported by Lim [37].

Different treatment methods corresponded to different infrared characteristic peaks. Comparing the regenerated PACs and the spent PAC, the peak intensities of benzene

C=C and phenyl Ar-H decreased and a carboxylic acid absorption peak of C=O, O-H appeared following regeneration, indicating that chemical bonds were ruptured in the structure of 4-CP after ultrasonic regeneration. Intermediate products with benzene rings and carboxylic acid were likely produced in the desorption process.

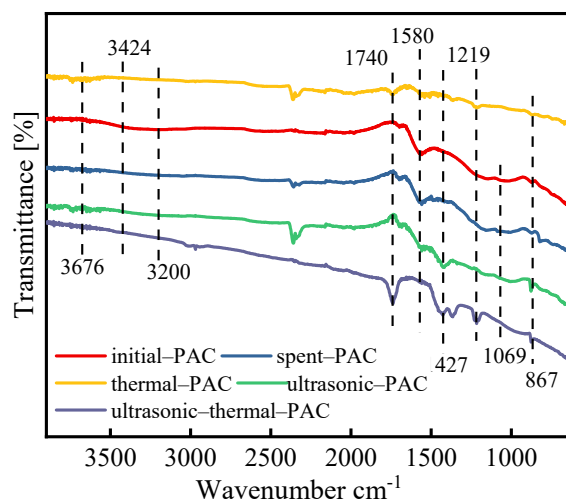


Figure 4. FTIR spectrum of different PACs.

3.3.2. Thermogravimetric Analysis

The TG and DTA trends from the thermogravimetric determination of PACs under different regeneration methods are displayed in Figure 5. As shown in Figure 5a, the thermal regeneration processes for various PACs are primarily separated into four separate phases: (i) the evaporation of water (under 150 °C); (ii) the pyrolyzation of small molecules on the PAC (150–260 °C); (iii) the elimination of the predominantly physically adsorbed substances from PACs (260–600 °C); (iv) the degradation of chemically adsorbed pollutants on PACs and the breaking of the chemical bonds of surface oxygen functional groups (at temperatures over 600 °C) [38]. In other researchers' reports, temperatures ranging from 40 to 200 °C were related to the desorption of weakly bonded water molecules adsorbed on the adsorbent [35]. Additional results show that temperatures of 250–350 °C are conducive to the oxidation and/or decomposition of chemical compounds strongly adsorbed in small pores [18]. Thus, for various adsorbates, the temperature for desorption was slightly different. The findings from Figure 5b show that there were noticeable variations in the DTA lines of the PACs, particularly in the third and fourth phases of the heating procedure. Regarding the DTA curve of the ultrasonic-thermal-PAC, there was an identifiable peak at 260 °C, but for the DTA curves of other regenerated PACs, there were no obvious peaks. This is due to the release of water vapor or the decomposition of other volatile substances on PAC. Another investigation also reported that in the chemical regeneration of spent PAC, the wide peak at temperatures above 650 °C may be due to the decomposition of surface functionalities [39]. The corresponding TG curve (Figure 5a) of ultrasonic-thermal-PAC decreased slowly as the PAC weight loss gradually increased. As reported, ultrasound would influence the surface functional groups of PAC, and functional groups such as C=O and O-H appeared after ultrasound regeneration [26]. This difference suggests that ultrasound treatment might weaken both physical interactions such as the Van der Waals force and the hydrogen bonding interaction between 4-CP molecules and the surface of PAC, which makes 4-CP easily desorbed by ultrasonic treatment and the following heat regeneration. It was observed that a peak emerged in the DTA curve of the ultrasonic-PAC between 260 and 650 °C, and a peak appeared in that of the thermal-PAC between 500 and 700 °C. Considering that the former peak was broader than the latter, it seems probable that there is no obvious separation between the third step and the fourth phase of the ultrasonic-PAC heating process. For the thermal-PAC, the TG curve displays a considerable drop in

the 400 °C to 800 °C temperature range, with a weight loss of 30.73%. This indicates that only thermal regeneration results in a high degree of PAC weight loss.

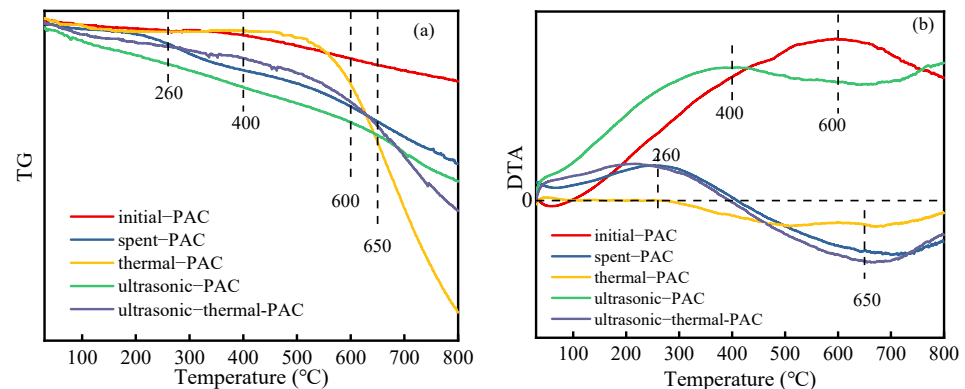


Figure 5. TG (a) and DTA (b) of different PACs.

3.3.3. Characterization of the Various PACs in Different Regeneration Processes

(1) Surface morphology

Several distinctions in the surface morphology of various PACs were predicted based on the SEM photographs. The graph of the initial PAC was smooth and flat, with no discernible contaminants (Figure 6a). Impurities were present on the spent PAC surface, and the impurities were aggregated (Figure 6b). Small holes appeared on the surface after a single thermal regeneration, with the PAC surface cleaned of contaminants (Figure 6c). Meanwhile, after a single ultrasonic treatment, several flaws and tunnels can be seen on the outer layer of the PACs (Figure 6d). The appearance of cracks and caves may be a result of the ultrasonic treatment's intense cavitation effect. After ultrasonic-thermal combined regeneration, there were some burr-like forms on the surface covered by a few impurities, which could be related to the organic cracking products on the carbon during the regeneration process (Figure 6e).

(2) XPS analysis

XPS spectra were used to study the elemental composition of the various regeneration treatments in more detail. The total survey spectra are presented (Figure S3); C and O could be detected. The obtained spectra were calibrated according to the C 1s peak (284.8 eV). The complex envelope in the high-resolution XPS spectra of the C 1s excitation suggests that several other carbon species were present on the surface of the PACs. The detailed scans of C 1s are displayed in Figure 7. Four signals used in the analysis of carbon material were included in the C 1s photoelectron spectrum of PAC [40–42]. The components were attributed to graphitic C atoms (C 1s (1)) [43], carbon entities in alcohol, ether groups and/or C–O–Cl bonds (C 1s(2), R–OH, C–O–C, C–O–Cl), carbon in hydroxyl groups (C 1s(3), C–OH), and carboxyl and/or ester groups (C 1s(4), O=C–OH, –C(O)–O–C) [43,44]. As can be seen from Figure 7, various regeneration processes produced different groups of C 1s. For thermal-PAC, the content of graphite carbon (area of peak C 1s (1)) decreased while the content of oxygenated carbon (area of peak C 1s (2)) increased, indicating some of the C was oxidized. For ultrasonic-PAC, the intensity of hydroxyl groups (area of peak C 1s (3)) increased, illustrating that ultrasound accelerated the generation of C–OH groups. Moreover, peak positions for the ultrasonic-PAC and ultrasonic-thermal-PAC were not significantly different, namely, the types of surface C 1s components were similar.

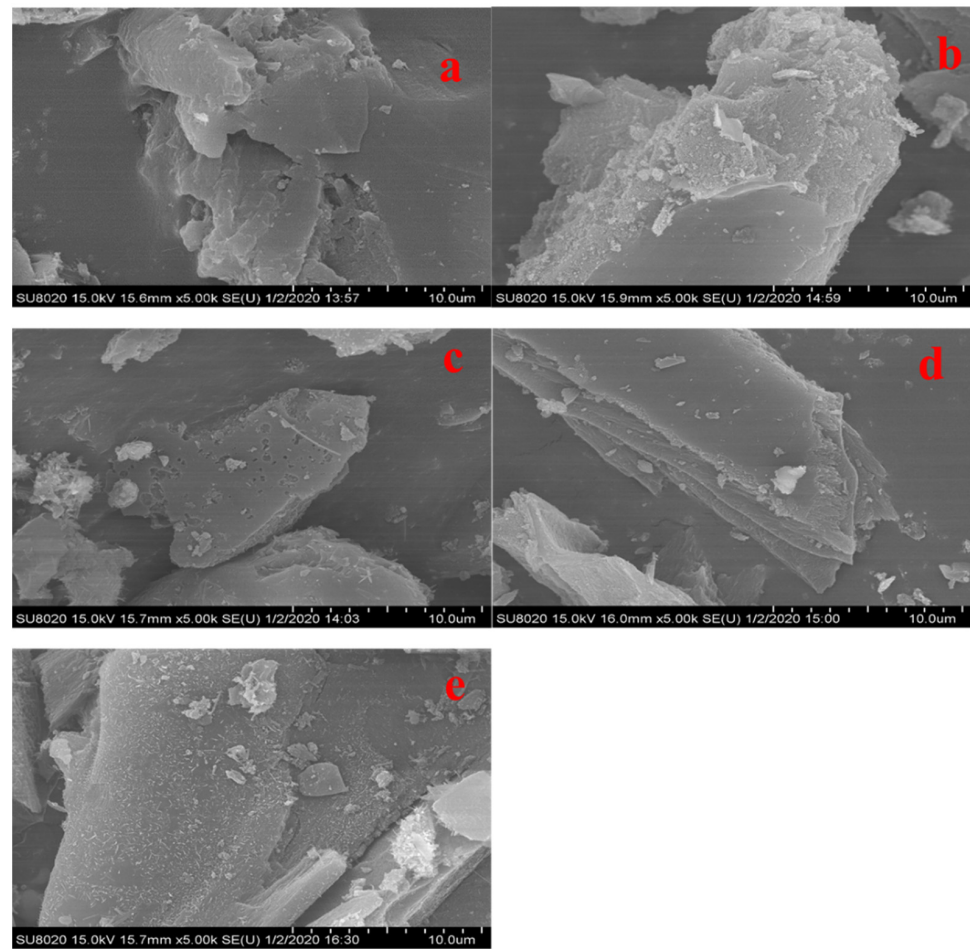


Figure 6. SEM of PACs with initial-PAC (a), spent-PAC (b), thermal-PAC (c), ultrasonic-PAC (d), and ultrasonic-thermal regeneration-PAC (e) (magnification 5000 times).

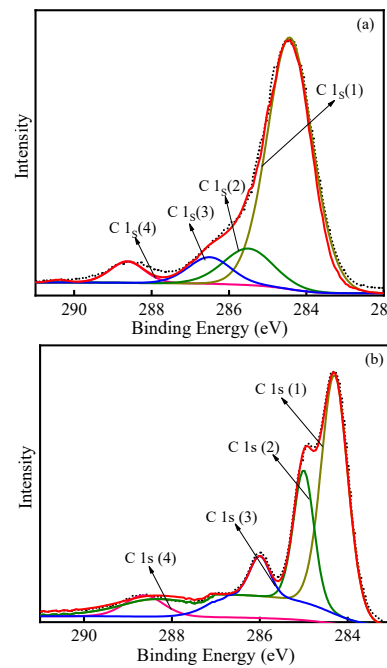


Figure 7. Cont.

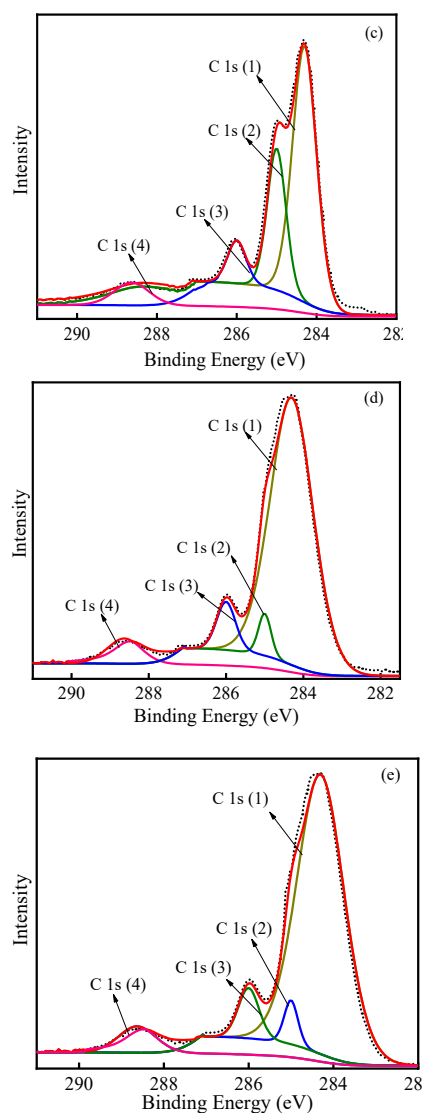


Figure 7. XPS spectra of C 1s in PAC with initial-PAC (a), spent-PAC (b), thermal-PAC (c), ultrasonic-PAC (d), ultrasonic-thermal-PAC (e).

The detailed scans of O 1s for various PACs are shown in Figure 8. The O 1s peaks were deconvoluted into 3–5 parts for the PACs. The O 1s (1) peak at 532.1–532.9 eV is attributed to singly bonded oxygen (–O–) in C–O [40,43]. The O 1s (2) peak at 531.1–531.5 eV is ascribed to –OH groups. The double bond connecting oxygen and carbon (C=O) in carbonyl and/or carboxyl is responsible for the O 1s (3) peak at 530.6–530.9 eV [45]. Moreover, the O 1s (4) peak at 533.3–533.6 eV is responsible for the chemisorbed oxygen and water. Obviously, there were differences in the oxygen forms of the PACs after various regeneration methods. The existence of various chemical states of oxygen is represented by the wide O 1s peaks. After thermal regeneration, the state of oxygen mainly was –O– in C–O. When the saturated PAC experienced ultrasonic irradiation, the states of oxygen mainly were C–O, –OH and double-bonded oxygen. In addition, for the ultrasonic-thermal-PAC, the form of oxygen mostly was double-bonded to carbon (C=O) in carbonyl and/or carboxyl, –OH groups and C–O. As presented in the XPS spectra, the oxygenous groups increased on the surface of the ultrasonic-thermal regenerated PAC. These oxygenous groups may affect the adsorption performance of the regenerated PAC and the subsequent adsorption-regeneration process.

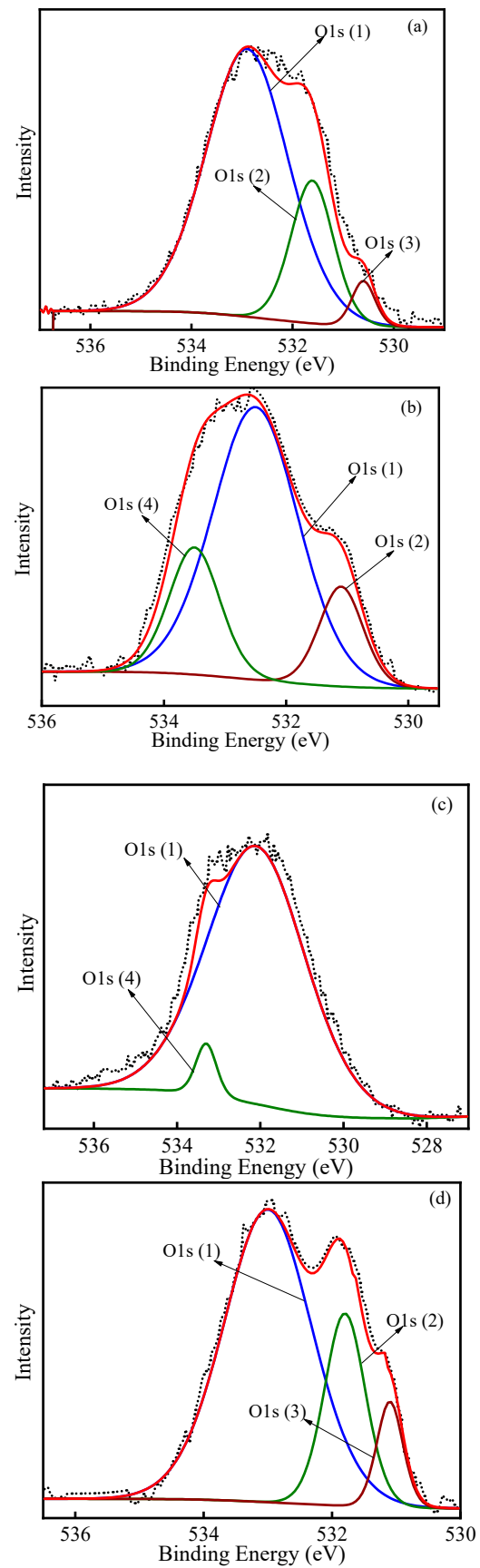


Figure 8. Cont.

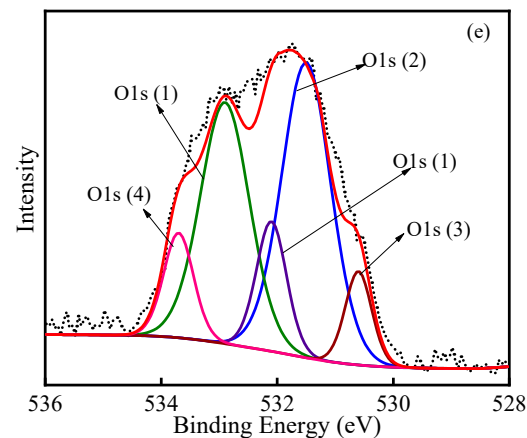


Figure 8. XPS spectra of O 1s in PAC with initial-PAC (a), spent-PAC (b), thermal-PAC (c), ultrasonic-PAC (d), ultrasonic-thermal-PAC (e).

(3) XRD analysis

XRD analysis was applied to explore the crystalline structure of several regenerated PACs, with outcomes recorded in Figure 9. We observed that the XRD peaks of the PACs were different after their regeneration processes. For all samples, the XRD diffraction peak of C (002) at 26.5° indicates a graphite structure for the carbon material [18,19,46–48], while a peak at 23.1° indicates amorphous carbon. The initial-PAC and spent-PAC displayed a wide and relatively high-intensity signal at 43° (100), which is assigned to the overlapped plane of graphite (PDF #41-1487) [18]. For ultrasonic-thermal-PAC, the peak at 31.7° (200) was related to carbon oxide (CO) and matched well with the standard card of PDF#74-1229. After the three regeneration treatments, the overlapped plane of graphite was significantly less present, demonstrating that the graphite structure of carbon can be slightly destroyed by both thermal regeneration and ultrasonic regeneration. In addition, the results show that the signal intensity of amorphous carbon with low crystallinity decreased, indicating that the effect of ultrasound and pyrolysis processes changed the crystal structure characteristics of the obtained carbons.

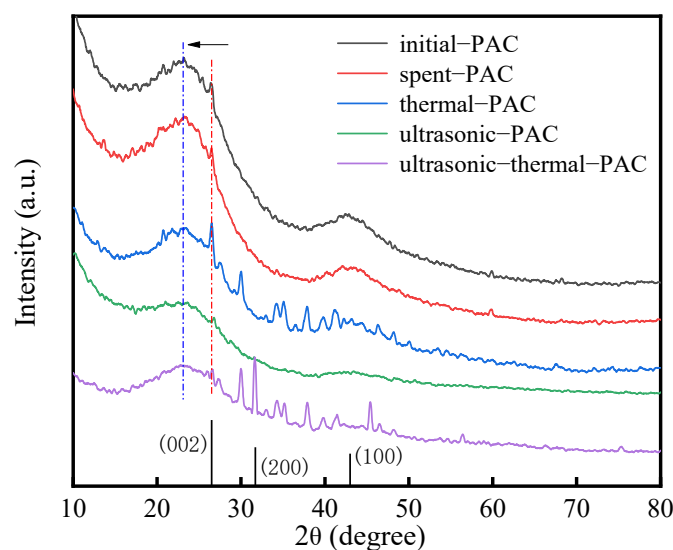


Figure 9. X-ray diffraction patterns of PACs.

4. Conclusions

In the present research, thermal treatment and a unique ultrasonic–thermal regeneration method were implemented to evaluate the regeneration of 4-CP spent PAC. The following conclusions can be derived from the results obtained:

- (1) Regarding single thermal regeneration processes, the RE and η values all improved with increases in regeneration temperature, heating rate and regeneration time. For practical treatment, we should select relatively reasonable parameters.
- (2) Under the optimum conditions for ultrasonic–thermal regeneration of PAC, a RE value of 90.99% and a η value of 5.6% were achieved. The results indicate that ultrasonic–thermal regeneration of PAC might be a practical and energy-efficient technique to reuse exhausted PAC.
- (3) The FTIR analysis and XPS results revealed that after ultrasonic–thermal regeneration, a considerable increase in oxygen-containing groups was observed. These oxygen-containing groups may affect the adsorption performance of the regenerated PAC and the subsequent adsorption–regeneration process. The thermogravimetric analysis indicated that ultrasound treatment might weaken the physical interaction force between 4-CP and PAC. Additionally, the XRD analysis demonstrated that the effect of ultrasound and pyrolysis processes changed the crystal structure characteristics of the obtained carbons.

Supplementary Materials: The following supporting information can be downloaded at: <https://www.mdpi.com/article/10.3390/su15119060/s1>, Figure S1: Effect of regeneration temperature on regeneration rate of PAC (a) regeneration time 30 min, (b) regeneration time 60 min; Figure S2: Effects of regeneration time on PAC regeneration rate and mass loss rate; Figure S3: The survey scan XPS spectrum of the PAC.

Author Contributions: Conceptualization, T.Z. and Y.Y.; methodology, T.Z.; software, T.Z.; validation, Y.Y. and Z.Z.; formal analysis, X.L.; investigation, B.W.; resources, X.L.; data curation, T.Z.; writing—original draft preparation, T.Z.; writing—review and editing, T.Z. All authors have read and agreed to the published version of the manuscript.

Funding: This research was funded by the Science and Technology Program of Gansu Province grant number (21JR7RA340).

Institutional Review Board Statement: Not applicable.

Informed Consent Statement: Not applicable.

Data Availability Statement: Data available on request due to restrictions eg privacy or ethical.

Acknowledgments: This study was financially supported by the Science and Technology Program of Gansu Province (21JR7RA340). The authors would like to express their gratitude for the peer review comments.

Conflicts of Interest: The authors declare no conflict of interest.

References

1. Derylo-Marczewska, A.; Sternik, D.; Swiatkowski, A.; Kusmierk, K.; Gac, W.; Buczek, B. Adsorption of phenol from aqueous and cyclohexane solutions on activated carbons with differentiated surface chemistry. *Thermochim. Acta* **2022**, *715*, 179299. [CrossRef]
2. Wei, X.; Huang, S.; Yang, J.; Liu, P.; Li, X.; Wu, Y.; Wu, S. Adsorption of phenol from aqueous solution on activated carbons prepared from antibiotic mycelial residues and traditional biomass. *Fuel Process. Technol.* **2023**, *242*, 107663. [CrossRef]
3. Lua, A.C. A comparative study of the pore characteristics and phenol adsorption performance of activated carbons prepared from oil-palm shell wastes by steam and combined steam-chemical activation. *Green Chem. Eng.* **2022**. [CrossRef]
4. Nabais, J.M.V.; Gomes, J.A.; Suhas; Carrott, P.J.M.; Laginhas, C.; Roman, S. Phenol removal onto novel activated carbons made from lignocellulosic precursors: Influence of surface properties. *J. Hazard. Mater.* **2009**, *167*, 904–910. [CrossRef] [PubMed]
5. Fagbohun, E.O.; Wang, Q.; Spessato, L.; Zheng, Y.; Li, W.; Olatoye, A.G.; Cui, Y. Physicochemical regeneration of industrial spent activated carbons using a green activating agent and their adsorption for methyl orange. *Surf. Interfaces* **2022**, *29*, 101696. [CrossRef]

6. Zhang, Q.; Zhang, M.; Li, T.; Du, R.; Yu, G.; Deng, S. FeOCl-confined activated carbon for improving intraparticle Fenton-like oxidation regeneration. *J. Hazard. Mater.* **2023**, *442*, 130026. [[CrossRef](#)]
7. Gazigil, L.; Er, E.; Yonar, T. Determination of the optimum conditions for electrochemical regeneration of exhausted activated carbon. *Diam. Relat. Mater.* **2023**, *133*, 109741. [[CrossRef](#)]
8. Li, J.; Zhou, W.; Su, Y.; Zhao, Y.; Zhang, W.; Xie, L.; Meng, X.; Gao, J.; Sun, F.; Wang, P.; et al. The enhancement mechanism of the microwave-assisted toluene desorption for activated carbon regeneration based on the constructive interference. *J. Clean. Prod.* **2022**, *378*, 134542. [[CrossRef](#)]
9. Xing, X.; Tang, J.; Yao, S.; Chen, H.; Zheng, T.; Wu, J. Electrochemical regeneration of granular activated carbon saturated by p-nitrophenol in BDD anode system. *Process. Saf. Environ.* **2023**, *170*, 207–214. [[CrossRef](#)]
10. Ren, M.; Wang, J.; Wang, Z.; Sun, S.; Qiu, J.; Shi, Y.; Wang, Z.-J.; Xie, Y. Activated carbon adsorption coupled with ozonation regeneration for efficient removal of chlorobenzene. *J. Environ. Chem. Eng.* **2022**, *10*, 107319. [[CrossRef](#)]
11. Bury, N.A.; Mumford, K.A.; Stevens, G.W. The electro-Fenton regeneration of Granular Activated Carbons: Degradation of organic contaminants and the relationship to the carbon surface. *J. Hazard. Mater.* **2021**, *416*, 125792. [[CrossRef](#)]
12. Leong, K.-Y.; Loo, S.-L.; Bashir, M.J.K.; Oh, W.-D.; Rao, P.V.; Lim, J.-W. Bioregeneration of spent activated carbon: Review of key factors and recent mathematical models of kinetics. *Chin. J. Chem. Eng.* **2018**, *26*, 893–902. [[CrossRef](#)]
13. Sun, Z.; Liu, C.; Cao, Z.; Chen, W. Study on regeneration effect and mechanism of high-frequency ultrasound on biological activated carbon. *Ultrason. Sonochem.* **2018**, *44*, 86–96. [[CrossRef](#)] [[PubMed](#)]
14. Chen, X.; Guo, Y.; Zhang, H.; Cheng, F.; Jiao, Z. Coke powder improving the performance of desulfurized activated carbon from the cyclic thermal regeneration. *Chem. Eng. J.* **2022**, *448*, 137459. [[CrossRef](#)]
15. Deng, H.; Cai, W.; Zhang, L.; Jia, Y.; Wang, X.; Zong, Q.; Cheng, G.; Hu, X.; Dong, C.; Zhao, Y. First kinetics verification of the useful H₂O gas inhibition on the thermal regeneration of spent activated carbon in flue gas desulfurization. *Fuel* **2023**, *337*, 126873. [[CrossRef](#)]
16. Guo, Y.; Du, E. The Effects of Thermal Regeneration Conditions and Inorganic Compounds on the Characteristics of Activated Carbon Used in Power Plant. *Energy Procedia* **2012**, *17*, 444–449. [[CrossRef](#)]
17. Márquez, P.; Benítez, A.; Chica, A.F.; Martín, M.A.; Caballero, A. Evaluating the thermal regeneration process of massively generated granular activated carbons for their reuse in wastewater treatments plants. *J. Clean. Prod.* **2022**, *366*, 132685. [[CrossRef](#)]
18. Márquez, P.; Benítez, A.; Hidalgo-Carrillo, J.; Urbano, F.J.; Caballero, A.; Siles, J.A.; Martín, M.A. Simple and eco-friendly thermal regeneration of granular activated carbon from the odour control system of a full-scale WWTP: Study of the process in oxidizing atmosphere. *Sep. Purif. Technol.* **2021**, *255*, 117782. [[CrossRef](#)]
19. Tan, L.; Wang, J.; Cai, B.; Wang, C.; Ao, Z.; Wang, S. Nitrogen-rich layered carbon for adsorption of typical volatile organic compounds and low-temperature thermal regeneration. *J. Hazard. Mater.* **2022**, *424 Pt A*, 127348. [[CrossRef](#)]
20. Zhou, E.; He, Y.; Ma, X.; Liu, G.; Huang, Y.; Chen, C.; Wang, W. Study of the combination of sulfuric acid treatment and thermal regeneration of spent powdered activated carbons from decolourization process in glucosamine production. *Chem. Eng. Process.* **2017**, *121*, 224–231. [[CrossRef](#)]
21. Shen, D.; Labreche, F.; Wu, C.; Fan, G.; Li, T.; Dou, J.; Zhu, J. Ultrasound-assisted adsorption/desorption of jujube peel flavonoids using macroporous resins. *Food Chem.* **2022**, *368*, 130800. [[CrossRef](#)]
22. Li, Z.; Xu, K.; Li, X.; Xi, H.; Hua, B.; Li, F. Effect of ultrasound on desorption kinetics of phenol from polymeric resin. *Ultrason. Sonochem.* **2006**, *13*, 225–231. [[CrossRef](#)]
23. Low, S.K.; Tan, M.C.; Chin, N.L. Effect of ultrasound pre-treatment on adsorbent in dye adsorption compared with ultrasound simultaneous adsorption. *Ultrason. Sonochem.* **2018**, *48*, 64–70. [[CrossRef](#)]
24. Hamdaoui, O.; Naffrechoux, E.; Tifouti, L.; Petrier, C. Effects of ultrasound on adsorption-desorption of p-chlorophenol on granular activated carbon. *Ultrason. Sonochem.* **2003**, *10*, 109–114. [[CrossRef](#)]
25. Lim, J.L.; Okada, M. Regeneration of granular activated carbon using ultrasound. *Ultrason. Sonochem.* **2005**, *12*, 277–282. [[CrossRef](#)]
26. Zhang, T.T.; Yang, Y.L.; Li, X.; Wang, N.; Zhou, Z.W. Regeneration of 4-chlorophenol from spent powdered activated carbon by ultrasound. *Environ. Sci. Pollut. Res.* **2019**, *26*, 9161–9173. [[CrossRef](#)]
27. Guilane, S.; Hamdaoui, O. Ultrasound-assisted regeneration of granular activated carbon saturated by 4-chlorophenol in batch-loop reactor. *Desalin. Water Treat.* **2016**, *57*, 17262–17270. [[CrossRef](#)]
28. Nunes, K.G.P.; Sfreddo, L.W.; Rosset, M.; Feris, L.A. Efficiency evaluation of thermal, ultrasound and solvent techniques in activated carbon regeneration. *Environ. Technol.* **2021**, *42*, 4189–4200. [[CrossRef](#)]
29. Kang, W.Z.; Li, Y.W. *Effect of Ultrasonic Treatment on the Nature of Regeneration of Activated Carbon*, 2nd ed.; China Energy Scientist Forum: Xuzhou, China, 2010; pp. 775–778.
30. Juang, R.S.; Lin, S.H.; Cheng, C.H. Liquid-phase adsorption and desorption of phenol onto activated carbons with ultrasound. *Ultrason. Sonochem.* **2006**, *13*, 251–260. [[CrossRef](#)]
31. Liu, C.; Sun, Y.; Wang, D.; Sun, Z.; Chen, M.; Zhou, Z.; Chen, W. Performance and mechanism of low-frequency ultrasound to regenerate the biological activated carbon. *Ultrason. Sonochem.* **2017**, *34*, 142–153. [[CrossRef](#)]
32. Shi, C.; Yang, W.; Chen, J.; Sun, X.; Chen, W.; An, H.; Duo, Y.; Pei, M. Application and mechanism of ultrasonic static mixer in heavy oil viscosity reduction. *Ultrason. Sonochem.* **2017**, *37*, 648–653. [[CrossRef](#)]

33. Chen, R.; Zheng, D.; Ma, T.; Ding, H.; Su, Y.; Guo, J.; Fu, H. Effects and mechanism of ultrasonic irradiation on solidification microstructure and mechanical properties of binary TiAl alloys. *Ultrason. Sonochem.* **2017**, *38*, 120–133. [[CrossRef](#)]
34. Ghaedi, H.; Ayoub, M.; Sufian, S.; Lal, B.; Uemura, Y. Thermal stability and FT-IR analysis of Phosphonium-based deep eutectic solvents with different hydrogen bond donors. *J. Mol. Liq.* **2017**, *242*, 395–403. [[CrossRef](#)]
35. Gabruś, E.; Tabero, P.; Aleksandrzak, T. A study of the thermal regeneration of carbon and zeolite adsorbents after adsorption of 1-hexene vapor. *Appl. Therm. Eng.* **2022**, *216*, 119065. [[CrossRef](#)]
36. Muncan, J.; Matovic, V.; Nikolic, S.; Askovic, J.; Tsenkova, R. Aquaphotomics approach for monitoring different steps of purification process in water treatment systems. *Talanta* **2020**, *206*, 120253. [[CrossRef](#)]
37. Lim, A.; Chew, J.J.; Ismadji, S.; Khaerudini, D.S.; Darsono, N.; Sunarso, J. Kinetic and equilibrium adsorption study of anionic dyes using oil palm trunk-derived activated carbon. *Mater. Today Proc.* **2022**, *64*, 1627–1638. [[CrossRef](#)]
38. Pastrana-Martinez, L.M.; Lopez-Ramon, M.V.; Moreno-Castilla, C. Adsorption and thermal desorption of the herbicide fluroxypyr on activated carbon fibers and cloth at different pH values. *J. Colloid Interface Sci.* **2009**, *331*, 2–7. [[CrossRef](#)]
39. Li, Q.; Qi, Y.; Gao, C. Chemical regeneration of spent powdered activated carbon used in decolorization of sodium salicylate for the pharmaceutical industry. *J. Clean. Prod.* **2015**, *86*, 424–431. [[CrossRef](#)]
40. Estrade-Szwarckopf, H. XPS photoemission in carbonaceous materials: A “defect” peak beside the graphitic asymmetric peak. *Carbon* **2004**, *42*, 1713–1721. [[CrossRef](#)]
41. Desimoni, E.; Casella, G.I.; Morone, A.; Salvi, A.M. XPS determination of oxygen-containing functional groups on carbon-fibre surfaces and the cleaning of these surfaces. *Surf. Interface Anal.* **1990**, *15*, 627–634. [[CrossRef](#)]
42. González-Elipse, A.R.; Martínez-Alonso, A.; Tascón, J.M.D. XPS characterization of coal surfaces: Study of aerial oxidation of brown coals. *Surf. Interface Anal.* **1988**, *12*, 565–571. [[CrossRef](#)]
43. Puziy, A.M.; Poddubnaya, O.I.; Socha, R.P.; Gurgul, J.; Wisniewski, M. XPS and NMR studies of phosphoric acid activated carbons. *Carbon* **2008**, *46*, 2113–2123. [[CrossRef](#)]
44. Fang, G.D.; Liu, C.; Gao, J.; Zhou, D.M. New Insights into the Mechanism of the Catalytic Decomposition of Hydrogen Peroxide by Activated Carbon: Implications for Degradation of Diethyl Phthalate. *Ind. Eng. Chem. Res.* **2014**, *53*, 19925–19933. [[CrossRef](#)]
45. Kannan, A.G.; Choudhury, N.R.; Dutta, N.K. Synthesis and characterization of methacrylate phospho-silicate hybrid for thin film applications. *Polymer* **2007**, *48*, 7078–7086. [[CrossRef](#)]
46. Bhadu, G.R.; Parmar, B.; Patel, P.; Paul, A.; Chaudhari, J.C.; Srivastava, D.N.; Suresh, E. Co@N-doped carbon nanomaterial derived by simple pyrolysis of mixed-ligand MOF as an active and stable oxygen evolution electrocatalyst. *Appl. Surf. Sci.* **2020**, *529*, 147081. [[CrossRef](#)]
47. Ni, J.; Huang, Y.; Gao, L. A high-performance hard carbon for Li-ion batteries and supercapacitors application. *J. Power Source* **2013**, *223*, 306–311. [[CrossRef](#)]
48. Xu, S.; Niu, M.; Zhao, G.; Ming, S.; Li, X.; Zhu, Q.; Ding, L.-X.; Kim, M.; Allothman, A.A.; Mushab, M.S.S.; et al. Size control and electronic manipulation of Ru catalyst over B, N co-doped carbon network for high-performance hydrogen evolution reaction. *Nano Res.* **2022**, *16*, 6212–6219. [[CrossRef](#)]

Disclaimer/Publisher’s Note: The statements, opinions and data contained in all publications are solely those of the individual author(s) and contributor(s) and not of MDPI and/or the editor(s). MDPI and/or the editor(s) disclaim responsibility for any injury to people or property resulting from any ideas, methods, instructions or products referred to in the content.